Soft Matter

Cite this: *Soft Matter*, 2011, **7**, 6135

www.rsc.org/softmatter

PAPER

A supramolecular structure with an alternating arrangement of donors and acceptors constructed by a *trans*-di-C_{60}-substituted Zn porphyrin derivative in the solid state†

Chien-Lung Wang,[a] Wen-Bin Zhang,[a] Chih-Hao Hsu,[a] Hao-Jan Sun,[a] Ryan M. Van Horn,[a] Yingfeng Tu,[b] Denis V. Anokhin,[c] Dimitri A. Ivanov[c] and Stephen Z. D. Cheng*[a]

Received 4th March 2011, Accepted 21st April 2011
DOI: 10.1039/c1sm05381g

When a molecule is constructed from geometrically isotropic [such as [60]fullerene (C_{60})] and anisotropic (such as porphyrin) units, as in the case of a *trans*-di-C_{60}-substituted Zn porphyrin derivative (diZnCPD), great interest lies in the understanding of their individual contributions to structural formations and phase transitions. For this purpose, the compound, diZnCPD, was designed and synthesized. Its phase behavior was investigated *via* differential scanning calorimetry (DSC) and polarized light optical microscopy (POM) and its supramolecular structure was elucidated *via* wide-angle X-ray diffraction (WAXD) and selective area electron diffraction (SAED) in transmission electron microscopy (TEM). The diZnCPD possesses a polymorphism in its ordered structures. When cooled from the isotropic (I) phase with experimentally accessible rates, instead of transferring into its ultimate stable phase, this compound formed a less ordered, metastable phase with a layered structure at 152 °C. Annealing this metastable phase enabled a further transformation into a stable phase with a higher transition temperature. As such, this metastable phase is monotropic. The formation of the stable phase was thus thermodynamically favorable, but kinetically more difficult (with a higher barrier for the transformation). Direct formation of this stable phase from the I state was unsuccessful even after prolonged isothermal experiments over several days above 152 °C, indicating that the formation barrier of this stable phase is extremely high. The thermally stable phase possessed a supramolecular structure with a triclinic unit cell of $a = 3.34$ nm, $b = 2.01$ nm, $c = 1.88$ nm, $\alpha = 89°$, $\beta = 98°$, and $\gamma = 90°$. Detailed structural analysis revealed that this is a donor–acceptor separated structure of C_{60}s and porphyrins nearly along the $[01\bar{1}]$ direction within which the zig-zag shaped C_{60} channels are along the [001] direction of the unit cell. We believe this is the first example of generating a donor–acceptor separated structure of C_{60}s and porphyrins in the bulk through a thermal annealing process. This structure provides promising potential for the use of this material to fabricate supramolecular electronic devices without utilizing a solvent process.

Introduction

π-Conjugated molecules have drawn significant attention in the emerging field of "plastic electronics" due to their useful optical, electronic properties and processibility.[1–4] Combining *p*-type and *n*-type π-conjugated molecules enables the photo-induced charge generation process and provide functions in applications such as photovoltaics and artificial photosynthesis.[5–19] In particular, using self-assembly to construct supramolecular structures of these π-conjugated molecules has been recognized as an important approach to generate "supramolecular electronics".[20–39] Research using [60]fullerene (C_{60}) as an electron acceptor (A) and porphyrin as an electron donor (D) has been extensively carried out. Most studies focus on the photo- and electronic properties in solution and/or solvent-induced supramolecular structures of C_{60}s and porphyrins. Materials containing C_{60} and porphyrin demonstrate an ability to efficiently harvest solar radiation and generate charge-separated states ($C_{60}^{-\cdot}$ and porphyrin$^{+\cdot}$) from photo-excited species.[40–44] Among all the structures, face-to-face aligned C_{60}-porphyrin dyads

[a]*Department of Polymer Science, College of Polymer Science and Polymer Engineering, The University of Akron, Akron, Ohio, 44325-3909, USA. E-mail: scheng@uakron.edu*
[b]*College of Chemistry, Chemical Engineering and Materials Science, Soochow University, Suzhou, 215123, China*
[c]*Institut de Sciences des Matériaux de Mulhouse, IS2M, CNRS LRC 7228, 15 Jean Starcky, F-68057 Mulhouse, France*

† Electronic supplementary information (ESI) available: ^{1}H NMR spectrum, ^{13}C NMR spectrum, MALDI-TOF mass spectrum, UV-Vis spectrum, and TGA diagram of diZnCPD. See DOI: 10.1039/c1sm05381g

demonstrated the fastest photon-induced charge separation process, which significantly surpass other relaxation processes such as fluorescence and intersystem crossing to the triplet state.[42] The supramolecular arrangement thus provides highly efficient photo-to-charge transformation. To utilize these physical properties of C_{60}-porphyrin derivatives, it is necessary to not only specifically design the chemical structures of the molecules but also carefully control over the hierarchical physical structures across multiple length scales. In such a way, transferring the intrinsic functions of the molecular structure into a desired macroscopic property becomes possible.

The supramolecular structures formed jointly by C_{60} and porphyrin are mainly reported as the products of co-crystallization of porphyrin derivatives and C_{60}.[45–52] Although delicate molecular designs provide the driving force for the structure formation, the formation of the structures normally requires a slow solvent evaporation process, and most of these solvent-included structures are unstable as the crystalline orders are gradually lost upon solvent removal. In addition, C_{60}s do not necessarily form a continuous phase in these structures due to the packing architecture of the host and the inclusion of solvent molecules. Therefore, developing readily processable and thermally stable supramolecular structures with face-to-face aligned porphyrins/C_{60}s is needed for practical applications.

Forming the supramolecular structures of C_{60} and porphyrin in the bulk is challenging due to the complexity of the phase formation in a system where C_{60}, which possesses an isotropic shape, prefers to form the plastic crystal phase,[53,54] and porphyrin, which possesses an anisotropic shape, prefers to form the columnar phase. It is known that C_{60} possesses strong, isotropic C_{60}–C_{60} interactions with each other.[55] On the contrary, porphyrin prefers one-dimensional disk-like interactions and stacks into a columnar structure.[56–59] In order to form a donor–acceptor separated structure, in addition to C_{60}–C_{60} and porphyrin–porphyrin interactions, the C_{60}–porphyrin interactions must also be taken into account for improving their optical and electronic performances. To the best of our knowledge, we are not aware of any reports on the formation of thermotropic supramolecular donor–acceptor separated structures of C_{60} and porphyrin formed in the solid state, especially without the assistance of solvent molecules and counter ions.

In this article, we report a thermally processable, stable, supramolecular structure with alternative stacking of C_{60}s and porphyrins formed by a *trans*-di-C_{60}-substituted Zn porphyrin derivative **1** (diZnCPD, Chart 1). When bearing two C_{60} moieties per molecule, the porphyrin–porphyrin interactions are no longer the dominating force to form the supramolecular structure of diZnCPD. It has been found that the C_{60}s and porphyrins are separately arranged nearly along the [01$\bar{1}$] direction while the zig-zag shaped C_{60} channels are along the [001] direction of the unit cell. The alkyl chains fill in the remaining space and allow the formation of the C_{60}–porphyrin supramolecular structure through a simple thermal process, which makes fabrication of large-area supramolecular electronics possible.

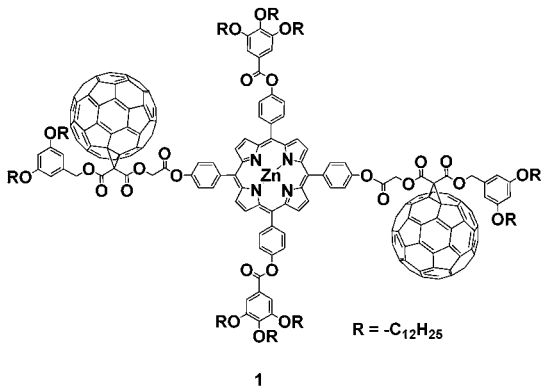

Chart 1 Molecular structure of diZnCPD (**1**).

Experimental

Materials

Unless otherwise noted, reagents and solvents were purchased as reagent grade and used without further purification. CH_2Cl_2 was purchased from Acros as anhydrous grade. 5,15-Di(*p*-hydroxyphenyl)-10,20-di[*p*-(3′,4′,5′-tris-dodecyloxybenzoyl-oxy)phenyl] Zn(II) porphyrin (**2**) and the carboxylic acid derivative of methanofullerene (**3**) were prepared according to the literatures.[57,60] Synthetic route of diZnCPD is shown in Scheme 1. The detail synthetic procedure and characterization data of diZnCPD are described below. The samples were kept in a vacuum before carrying out characterization and analysis.

Synthesis of diZnCPD (1)

3 (274 mg, 2.0×10^{-1} mmol), **2** (200 mg, 9.7×10^{-2} mmol), and 4-(dimethylamino) pyridinium toluene-*p*-sulfonate (DPTS, 72 mg, 2.4×10^{-1} mmol) were dissolved in CH_2Cl_2 (40 mL), and cooled to 0 °C. *N*,*N*′ Diisopropyl-carbodiimide (DIPC, 37 mg, 3.0×10^{-2} mmol) was slowly added into the solution by a microsyringe. The solution was stirred at room temperature for 2 day. The solvent was then evaporated by a rotary evaporator under reduced pressure. The residue was dissolved in CH_2Cl_2, and subjected to column chromatography (SiO_2, CH_2Cl_2) to allow isolation of **1**. The obtained dark brown fraction was then concentrated. The product was re-precipitated into acetone as a black solid (435 mg). Yield: 91%.

^{1}H NMR (300 MHz, $CDCl_3$): δ (ppm) 9.02 (d, $J = 4.5$ Hz, 4H), 8.95 (d, $J = 4.5$ Hz, 4H), 8.29–8.22 (m, 8H), 7.66–7.57 (m, 12H), 6.67 (d, $J = 1.8$ Hz, 4H), 6.44 (br s, 2H), 5.54 (s, 4H), 5.36 (s, 4H), 4.18–4.11 (12H, m), 3.93 (t, $J = 6.3$ Hz, 8H), 1.93–1.71 (m, 20H), 1.58 (br s, 12H), 1.30–1.21 (m, 168H), 0.91–0.83 (m, 30H). ^{13}C

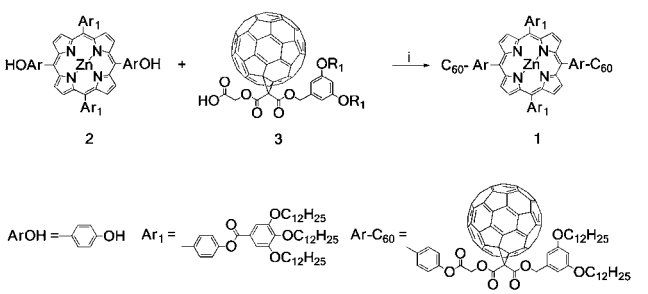

Scheme 1 Synthetic route of diZnCPD (**1**). *Reagents and conditions*: (i) *N*,*N*′-diisopropyl-carbodiimide (DIPC), 4-(dimethylamino) pyridinium toluene-*p*-sulfonate (DPTS), CH_2Cl_2, 25 °C, 2 days.

NMR (75 MHz, $CDCl_3$): δ (ppm) 165.5, 165.4, 163.4, 163.2, 160.8, 153.3, 151.2, 150.6, 150.4, 150.1, 145.3, 145.2, 145.1, 145.0, 144.9, 144.8, 144.7, 143.9, 143.9, 143.5, 143.1, 143.0, 142.2, 142.0, 141.9, 141.2, 141.1, 141.0, 140.4, 139.7, 139.0, 136.8, 135.5, 124.3, 120.7, 120.2, 119.7, 109.1, 107.6, 105.3, 73.9, 71.4, 69.6, 69.5, 68.5, 63.1, 32.2, 32.1, 30.6, 30.0, 30.0, 29.9, 29.9, 29.8, 29.7, 29.6, 29.6, 29.5, 26.4, 26.3, 22.9, 22.9, 14.4, 14.3. MALDI-TOF mass: calcd for $C_{322}H_{292}N_4O_{26}Zn$ $[M]^+$: $m/z = 4694.10$; found $[M]^+$: $m/z = 4694.77$.

Sample preparation

For differential scanning calorimetry (DSC) experiments, about 5.0 mg of sample was used and the reference and sample pan weights were kept constant with a precision of ± 0.001 mg. Samples for one-dimensional (1D) wide-angle X-ray diffraction (WAXD) measurements were prepared by melting the sample on an aluminium substrate to obtain a 0.5 mm thick film. The phase transitions and their corresponding phase structural transformations were monitored by DSC and 1D WAXD experiments in the following three thermal processes. First, the samples were first heated to 200 °C to eliminate their previous thermal history, and the subsequent cooling and heating experiments at a scan rate of 5 °C min^{-1} in DSC and 1D WAXD were then recorded. Second, the samples were first heated to 200 °C, subsequently cooled to 145 °C and then annealed at 145 °C for 3 days, followed by cooling to 30 °C in a Mettler hot stage (FP-90). The heating DSC and 1D WAXD experiments at a scan rate of 5 °C min^{-1} were then recorded for the samples. Third, the samples were first heated to 200 °C and then cooled to 155 °C, and annealed at 155 °C for 4 days. The samples were then directly heated from 155 °C to 200 °C at a scan rate of 5 °C min^{-1}, and the heating DSC and 1D WAXD experiments were recorded.

The diZnCPD samples for 2D WAXD experiments were prepared by mechanically extruded diZnCPD films at 120 °C after being directly cooled from 200 °C between two aluminium sheets. The samples were then annealed at 145 °C for 3 days before the experiments were conducted.

To conduct the selective area electron diffraction (SAED) experiments and investigate the morphology of diZnCPD in the nanometre scale, transmission electron microscopy (TEM) samples were prepared by first solution-casting a 0.01% (w/v) CH_2Cl_2 solution of diZnCPD on carbon-coated mica surfaces. The sample thermal histories were also identical to those in the DSC and 1D WAXD experiments. After the thermal treatment process, the samples were removed from the mica surface and collected on copper grids.

For the observation of the morphology in the micrometre scale and birefringence of the diZnCPD sample in polarized light optical microscopy (POM) experiments, the diZnCPD samples were prepared by solution-casting a 0.1% (w/v) CH_2Cl_2 solution of diZnCPD on glass slides. Again, the thermal histories were the same as those in DSC and 1D WAXD experiments. The samples used for POM had a typical thickness of 5 μm.

Instrumentation

^1H and ^{13}C NMR spectra were obtained with a Varian Gemini 300 NMR at 300 and 75 MHz, respectively. ^1H NMR spectra were referenced to the residual proton impurities in the $CDCl_3$ at δ 7.27 ppm. ^{13}C NMR spectra were referenced to $^{13}CDCl_3$ at δ 77.00 ppm. Matrix-assisted laser desorption/ionization-time of flight (MALDI-TOF) measurements were carried out on a Bruker Ultraflex III TOF (Bruker Daltonics, Inc., Billarica, MA), equipped with a Nd:YAG laser emitting at a wavelength of 355 nm. All spectra were measured in the positive reflector mode. The instrument was calibrated prior to each measurement with external standards, poly(methyl methacrylate) and polystyrene. Data analysis was carried out on the software of flexAnalysis.

The thermal properties of the phase transitions were characterized with a Perkin-Elmer PYRIS Diamond differential scanning calorimeter with an Intracooler 2P apparatus. The temperature and heat flow scales were calibrated at different heating and cooling rates (1–40 °C min^{-1}) using standard materials. Transition temperatures were determined using the onset temperatures. An onset temperature was defined by the cross-point of the peak slope and the baseline in the DSC diagrams. Upon cooling, the onset temperature was determined on the high-temperature side, and upon heating the onset temperature determined was on the low-temperature side. The thermogravimetric measurements were conducted on a TA TGA Q500 instrument at 10 °C min^{-1} in a nitrogen atmosphere.

The structural changes with temperature were detected using 1D WAXD patterns obtained with a Rigaku Multiflex 2 kW Automated Diffractometer using Cu K_α radiation (0.1542 nm). A hot stage was installed on the diffractometer to study phase structure transitions as a function of temperature. The hot stage was calibrated with a deviation within ±0.5 °C. The samples were scanned in reflection across a 2θ range of 1.8–40° at a 1° per min rate. For the structure determination, 2D WAXD experiments on mechanically extruded diZnCPD samples were performed on a custom-built WAXD instrument coupled to a Rigaku MicroMax™-007 HF rotating anode generator (again, Cu K_α radiation). The data were collected using X-ray sensitive Fuji image plates with a pixel size of 100 × 100 μm^2. The modulus of the scattering vector s was calibrated using several diffraction orders of silver behenate in the low-angle region ($2\theta < 15°$), and silicon crystals in the high-angle region ($2\theta > 15°$). 2D WAXD experiments were also conducted on a Rigaku 18 kW rotating anode X-ray generator attached to an R-AXIS-IV image plate system. The crystal unit cells were determined by constructing reciprocal lattices. Computer refinement was conducted to find the solutions with the least error between the calculated values and the experimental results.[61,62]

TEM experiments were carried out with a Philips Tecnai 12 using an accelerating voltage of 120 kV. SAED patterns were obtained using a TEM tilting stage to determine the crystal structure parameters. The d-spacings were calibrated using a TlCl standard. Morphological observations at micrometre scale were conducted using a POM (Olympus BH-2) coupled with a Mettler hot stage (FP-90).

Computer molecular modeling and analysis of the diffraction patterns were performed using the Cerius^2 package of Accelrys. Basic unit cell parameters determined by crystallographic experimental data from the 2D WAXD and SAED experiments were used to build the crystal unit cell.

Results and discussion

Synthesis of diZnCPD

The diZnCPD molecule was synthesized by reacting 5,15-di-(*p*-hydroxyphenyl)-10,20-di[*p*-(3′,4′,5′-tris-dodecyloxy benzoyloxy)phenyl] Zn(II) porphyrin with a carboxylic acid derivative of methanofullerene using Steglich esterification. The products were characterized by ^{1}H NMR, ^{13}C NMR, MALDI-TOF mass spectrometry (Fig. S1†), and UV-Vis spectroscopy (Fig. S2†) to confirm their chemical identity and purity. The Steglich esterification provides an excellent yield (91%) in the synthesis of diZnCPD. This compound is black in color and exhibits crystalline phases at room temperature. Good thermal stability was observed from the thermogravimetric analysis (Fig. S3†). The 1% weight loss temperature of diZnCPD is at 303 °C when the heating rate was at 10 °C min^{-1} in N_2. The supramolecular structure of diZnCPD in the bulk was then elucidated by a combined technique of DSC, WAXD, and SAED in TEM.

Phase behaviors of diZnCPD

Fig. 1a shows a set of DSC cooling and subsequent heating thermal diagrams of diZnCPD at a scan rate of 5 °C min^{-1}. This compound exhibits only one transition process occurring at an onset temperature of around 152 °C during both cooling and subsequent heating with an identical heat of transition of 4.7 kJ mol^{-1}. Above this temperature, the compound enters the isotropic (I) phase, as confirmed by WAXD and POM experiments (*vide infra*). However, the heating thermal diagram of diZnCPD after being cooled from the isotropic melt to 120 °C and annealed at 145 °C for 3 days and then further cooled to room temperature (Fig. 1b) shows a new transition process at an even higher temperature of around 170 °C, with a higher heat of transition of 34.7 kJ mol^{-1}. Therefore, the phase behavior of this compound is monotropic.[63–68] Since this transition exhibits a much higher transition enthalpy occurring at the higher temperature, we expect that the phase with a transition temperature at 170 °C must possess a higher order and thus it is a more stable phase. Furthermore, the phase occurred at 152 °C must have a less ordered structure, and it is actually a metastable phase compared with the stable phase. The appearance of this less ordered phase in Fig. 1a is due to the fact that the formation kinetics of the higher ordered, stable phase is extremely slow (with a very high transition barrier) and can be bypassed under a cooling and heating rate of 5 °C min^{-1}.

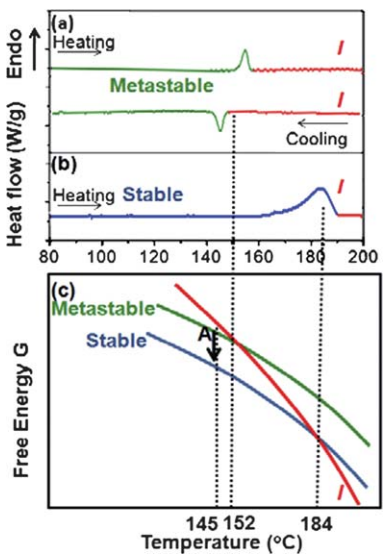

Fig. 1 DSC thermal diagrams of diZnCPD at a scan rate of 5 °C min^{-1}. (a) Cooling diagram from the I phase and the subsequent heating curve and (b) heating diagram of the sample after annealed at 145 °C for 3 days. (c) Schematic illustration of the free energies of the stable, metastable and isotropic states of diZnCPD with respect to temperature at atmospheric pressure. The "A" represents the annealing process.

This phase stability relationship can be illustrated in Fig. 1c in terms of the diagram between free energies of the metastable, stable and I phases with respect to temperature at atmospheric pressure.[63–68] At high temperatures, much higher than 170 °C, the I phase is the most stable phase. During the cooling, the stable ordered phase should first form from the I phase. However, the barrier in forming this stable ordered phase is so high that a cooling rate of 5 °C min^{-1} is not slow enough to allow the compound to develop this ordered phase. In fact, at the slowest cooling rate we used (1 °C min^{-1}) or even when isothermally held at a temperature higher than 152 °C for several days, the formation of this stable phase did not take place. Instead, the I to metastable phase transition occurred at around 152 °C with a heat of transition of 4.7 kJ mol^{-1} during the cooling at −5 °C min^{-1}. This metastable phase melts, in the subsequent heating, at 152 °C with an identical heat of transition, revealing that the metastable phase is a liquid crystal-like phase for which the transition usually does not exhibit supercooling in transition temperature.[14,17] Formation of the stable phase requires long thermal annealing, such as annealing the metastable phase at 145 °C for 3 days.

To study the corresponding structural change during the thermal processes and identify the phase structures of the metastable and stable phases, Fig. 2a shows a series of one-dimensional (1D) WAXD patterns during cooling according to the DSC results. The I phase is confirmed by the amorphous halos at 2θ values of 2.4° and 19.6° in the pattern recorded at 155 °C. The halo at the high 2θ angle represents a short-range order at the segmental scale within the molecules; meanwhile, the halo with the low 2θ angle can be attributed to the short-range order between the whole molecules. In the 1D WAXD pattern recorded at 120 °C (in fact, when the temperature is slightly below 152 °C, the same pattern can be seen), a single sharp reflection peak with a *d*-spacing = 3.77 nm and an amorphous halo at 19.6° is observed, representing a feature of the metastable phase formation. The *d*-spacing of the diffraction peak decreases slightly to 3.72 nm when cooled to 35 °C due to the thermal shrinkage. During the subsequent heating, the *d*-spacing of the diffraction peak returns back to 3.77 nm at 120 °C, and then the metastable phase directly enters the I phase as indicated by the two amorphous halos in the pattern at 155 °C. Fig. 2b shows multiple diffraction peaks, indicating the formation of the ordered stable phase after annealing the sample at 145 °C for 3 days. The diffraction pattern remains above 152 °C, the transition temperature of the metastable phase to the I phase. Only after around 180 °C is reached, can the diffractions disappear and the I phase be reached. Therefore, the WAXD results also

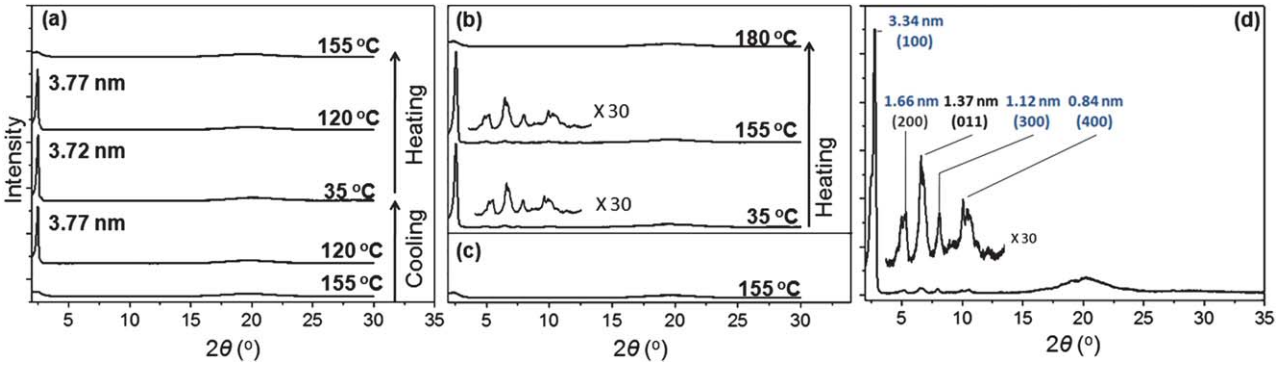

Fig. 2 Set of 1D WAXD patterns of diZnCPD (a) for the cooling process from the I phase and the subsequent heating process, (b) for the heating process after annealing at 145 °C for 3 days and cooled to 30 °C before recording the patterns, (c) obtained at 155 °C after cooling from the I phase and annealing at 155 °C for 4 days, and (d) indexes of the 1D WAXD pattern of diZnCPD obtained after annealing at 145 °C for 3 days and cooled to 30 °C before the experiments.

support the observation of polymorphism and phase behavior of the diZnCPD analyzed based on the DSC observations.

However, this ordered stable phase cannot be formed when the sample was directly cooled to a temperature above 152 °C. As shown in Fig. 2c, after the sample was cooled from 200 °C and isothermally held at 155 °C for 4 days, the 1D WAXD pattern recorded at 155 °C still remains identical to that recorded in the I phase. This again supports the conclusion based on the DSC experiments that the ordered stable phase is extremely difficult to form in such a high temperature region (with a very high barrier). Nevertheless, a two-step ordering process, including the I phase to the metastable phase and the metastable phase to the stable phase transitions, allows diZnCPD to overcome the energy barrier in a stepwise pathway and makes the formation of the stable phase kinetically possible. Therefore, the metastable phase plays an important role as a precursor in the formation of the ordered stable phase.

Fig. 2d is the 1D WAXD pattern of the diZnCPD sample after annealing at 145 °C for 3 days and cooled to 30 °C. The diffraction peaks of this stable phase were enlarged as an inset in Fig. 2d. Five reflection peaks with *d*-spacings of 3.34, 1.66, 1.37, 1.12, and 0.84 nm can be observed. Among them, diffraction peaks with *d*-spacing of 3.34, 1.66, 1.12, and 0.84 nm possess *q* ratios of 1 : 2 :3 : 4. We speculate that this ordered structure may possess a layered structure. However, precise determination requires a 2D WAXD pattern to illustrate the dimensionality of the ordered structure. The indexes of Fig. 2d were obtained after the 2D WAXD and SAED results were analyzed.

Phase structure determinations of diZnCPD

A 2D WAXD pattern of fibers of the stable phase is shown in Fig. 3a. The sample was extruded in the metastable phase at 120 °C after heating to 200 °C, and then annealed at 145 °C for 3 days. The (100), (200), (300) and (400) diffractions are observed along the equator with the *d*-spacings of 3.34, 1.66, 1.12, and 0.84 nm, respectively, which are identical to those shown in the 1D WAXD pattern of Fig. 2d. Along the meridian direction, two pairs of diffractions, with *d*-spacings of 2.01 and 1.01 nm, can be observed. We assign them as the (010) and (020) diffractions. However, the azimuthal intensity profiles of the off-meridional peaks indicate that the texture of the material is not identical to the conventional fiber symmetry. Indeed, in this case the layers are parallel to the extrusion direction with the a^* axis rotating in the plane perpendicular to the fiber axis and the *bc* plane of the lattice, which is parallel to the layer planes, freely rotating along the a^* axes (a more detailed description can be found in ref. 69). The observed biaxial texture of the fiber in the stable crystalline phase probably results from the orientation of the parent metastable liquid-crystalline phase.[70] In Fig. 3a, a pair of diffractions that are slightly above the (010) and deviates from the meridian cannot be incorporated into the a^*b^* reciprocal lattice, and should be assigned as the (001) diffraction. The indexes of both (010) and (001) can be further confirmed by the SAED pattern along the [100] zone in Fig. 3b, which clearly shows the b^*c^* reciprocal lattice. Furthermore, because the α^* angle is 91° in the b^*c^* reciprocal lattice, the α angle can be determined as 89°. With the 2D WAXD and SAED patterns, the lattice parameters can be determined as $a = 3.34$ nm, $b = 2.01$ nm, $c = 1.88$ nm, $\alpha = 89°$, $\beta = 98°$, and $\gamma = 90°$. The unit cell of the stable phase of diZnCPD is thus triclinic. With these unit cell parameters, the remaining one strong reflection observed in the 1D WAXD

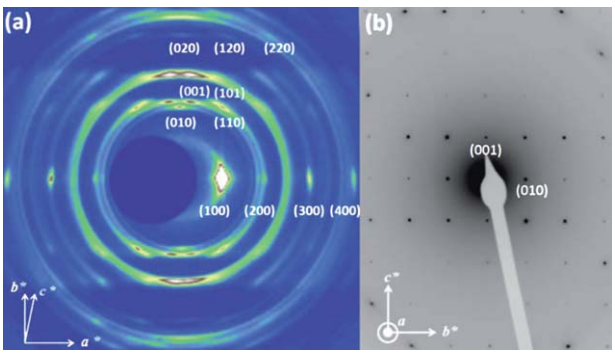

Fig. 3 (a) 2D WAXD pattern and (b) SAED along [100] zone of the stable phase of diZnDCP. The sample used in this 2D WAXD experiment was extruded at 120 °C after heated to 200 °C, and annealed at 145 °C for 3 days before recording the pattern. The sample used in the SAED experiment was solvent cast and heated to 200 °C, cooled to 120 °C and then annealed at 145 °C for 3 days before recording the pattern.

pattern in Fig. 2d with a *d*-spacing of 1.37 nm can be assigned as the (110) diffraction.

Calculations based on the molecular weight of diZnCPD (4694.09 g per mole = 0.780×10^{-20} g per molecule) and the unit cell volume (1.252×10^{-20} cm^3) give a theoretical density with two molecules per unit cell of 1.24 g cm^{-3}. This density matches well with the measured density, 1.23 g cm^{-3}.

To further investigate the structure of the metastable phase, Fig. 4 shows a set of 2D WAXD patterns of this phase. The sample was melted at 200 °C, sheared at 120 °C and then cooled to room temperature at 5 °C min^{-1}. A pair of strong diffractions with a *d*-spacing of 3.72 nm is observed when the incident X-ray beam is along the front direction (FD) or shear direction (SD) of the sample (see the inset of the sheared geometry of this figure), as shown in Fig. 4a and c. On the other hand, a very weak diffraction ring with the same *d*-spacing is also seen when the incident X-ray beam is along the through direction (TD, Fig. 4b), which probably results from a trace amount of randomly oriented fraction in the sample. The result indicates that the metastable phase may also possess a layered structure and the mechanical shearing direction is parallel to the layer interfaces, and perpendicular to the normal direction of the layers (and thus, the normal direction of the substrate). The single diffraction pair without high order diffractions may indicate that this layered structure is at most in a quasi-long range order. This structure characterization indicates that the kinetically favorable metastable phase is a low-order liquid crystalline phase with a smectic arrangement.[71] This layered metastable phase serves as a precursor of the triclinic stable phase in such a way that the layered structure is aligned with the (100) planes of the triclinic phase.

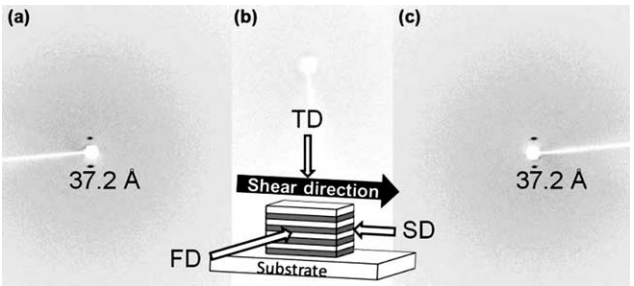

Fig. 4 2D WAXD patterns of the metastable phase of diZnCPD with incident X-ray beam direction along (a) the front direction (FD), (b) the through direction (TD) and (c) shear direction (SD). The solid arrow indicates the direction of mechanical shearing force applied on the sample. The hollow arrows indicate the direction of the incident X-ray beam.

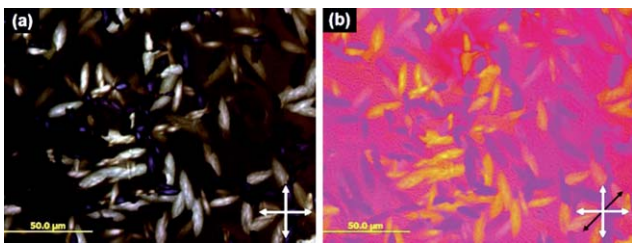

Fig. 5 Room temperature POM images of the stable phase of diZnCPD: (a) without tint plate and (b) with tint plate. The white cross in the right bottom of the images indicates the polarization directions of the analyzer and the polarizer in the microscopy. The black arrow in (b) indicates the slow axis of the tint plate.

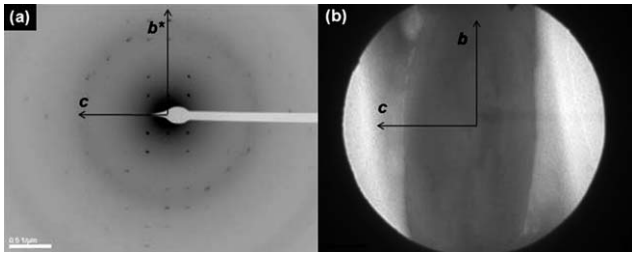

Fig. 6 (a) SAED pattern and (b) corresponding TEM image of the stable phase of diZnCPD.

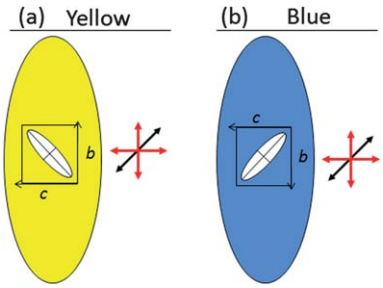

Fig. 7 Illustrations of the relative orientation of the birefringence ellipsoid (on the *bc*-plane) and the slow axis of the tint plate. Under POM, olive-shaped morphology would appear yellow in arrangement (a) and it would appear blue in arrangement (b). The red-cross indicates the polarization directions of the analyzer and the polarizer in POM. The black arrow indicates the slow axis of the tint plate. The outer ellipsoid illustrates the olive-shaped morphology and the inner ellipsoid represents the birefringence ellipsoid in a unit cell.

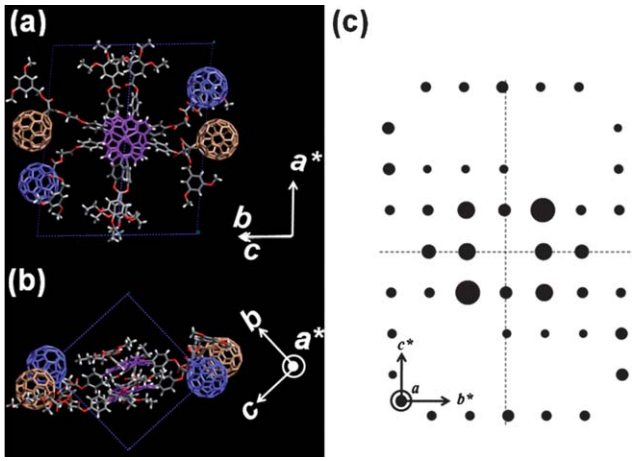

Fig. 8 Energy-minimized models of the stable phase of diZnCPD. (a) Illustration of the motif in the unit cell viewed along [0$\bar{1}$1] zone. The motif is constructed with 2 molecules of diZnCPD. (b) Illustration of the motif in the unit cell viewed along the *a** axis. (c) The simulated [100] zone ED pattern generated based on the constructed molecular packing model. The models are built based on molecular mechanics simulation and the experimental diffraction data.

Fig. 5 shows the phase morphologies of the stable phase of diZnCPD observed under POM. The stable phase shows a birefringent olive-shaped morphology. An important feature in the POM images is that the olive-shaped morphology is the brightest when its long axis is parallel to the polarization direction of the analyzer or the polarizer (Fig. 5a). After the tint plate was applied (Fig. 5b), yellow and blue colors were observed on the olive-shaped morphology. In order to correlate the birefringence with the crystal structure, Fig. 6 shows a SAED pattern (Fig. 6a) and a corresponding bright field TEM image of the olive-shaped phase morphology (Fig. 6b). The SAED pattern in Fig. 6a indicates that the long axis and short axis of the olive-shaped morphology correspond to the *b*- and *c*-axes of the stable phase. Therefore, the long axis of the birefringence ellipsoid on the *bc*-plane of the unit cell is not parallel to either the *b*- or *c*-axis. The colors in Fig. 5b result from the relative orientation between the birefringence ellipsoid and the slow axis of the tint plate, as indicated in Fig. 7. Fig. 5b also supports the fact that the ellipsoid is tilted away from the *b*- and *c*-axes. Therefore, all of these results indicate that along the [100] zone, the long axis of the motifs has to tilt away from the *b*- and *c*-axes.

Molecular packing of the stable phase

Fig. 8 shows the energy-minimized model and a simulated ED pattern of the stable phase of diZnCPD. The unit cell is built based on the unit cell parameters determined from the diffraction experiments, and the motif is constructed by two diZnCPD molecules based on the density calculation. The formation of the motif is identified to be driven by the π–π interaction of the two Zn(II) porphyrins, which can be clearly seen in Fig. 8a and b. These two Zn(II) porphyrins are co-planar and have a rotational angle of 25° along the porphyrin normal, as shown in Fig. 8a. Each porphyrin possesses two C_{60}s. In Fig. 8a, the two C_{60}s colored in blue are connected with one porphyrin, and those colored in brown are with another porphyrin. In Fig. 8b, the C_{60}s colored in brown are in the same *bc*-plane. The left side C_{60} colored in blue is beneath the brown C_{60}, yet the right side C_{60} colored in blue is above the C_{60} colored in brown. This porphyrin–porphyrin interaction leads to a geometry wherein these two molecules are more or less within a sheet-like structure. The normal of this sheet-like structure is close to being within the *bc*-plane, namely, the sheet-like structure is nearly perpendicular to the *bc*-plane. Furthermore, this sheet-like structure is located more or less along the diagonal direction of the *bc*-plane of the unit cell (Fig. 8b). The expected birefringence generated by this motif arrangement also matches the POM observation. The simulated [100] zone ED pattern is shown in Fig. 8c based on this constructed molecular packing model. This ED pattern nearly matches the experimental ED pattern as shown in Fig. 3b, indicating the molecular arrangement in the model is close to the real structure of the stable phase of diZnCPD.

Fig. 9 shows a space-filling molecular model with 3 × 3 unit cells viewed along the *a**-axis, where the projection of the *bc*-plane is seen. In Fig. 9a, the position of a motif is indicated by the yellow parallelogram, which is the same as shown in Fig. 8b. The motif arrangement in this figure allows two of the four C_{60}s (colored in brown) to adapt the positions on the top and bottom of the Zn(II) porphyrin cores in the neighboring motif, as indicated by the red rectangles. Therefore, the C_{60}s (acceptors) and porphyrins (donors) can form this close packing along the direction near to the [01$\bar{1}$] direction of the unit cell, which is better visualized in Fig. 9b. In this figure, the C_{60}s colored in blue, which are above and beneath of the *bc*-plane, and the alkyl chains are removed. The green rectangle in Fig. 9b clearly shows the packing of 2C_{60}s at the top and bottom of 2Zn(II) porphyrins, which results in that particular motif orientation in the unit cell. In Fig. 9a, the remaining two C_{60}s (colored in blue) of a moiety in the yellow parallelogram occupy the empty space created by the two bulky brown C_{60}s in the stack, and the dodecyl chains may further encapsulate and stabilize the whole supramolecular structure. The obtained structure is therefore thermally stable and solvent-molecule-free.

Another important feature in this structure is a contacting zig-zag packing scheme for constructing the C_{60} channels along the [001] direction. By omitting the non-C_{60} moieties in Fig. 9a, Fig. 9c clearly shows the packing of C_{60}s in the structure. The center-to-center distances between the neighboring brown C_{60}s are 1.0 and 1.1 nm, and the neighboring brown and blue C_{60}s are 1.0 nm apart, which is close to the center-to-center distance of

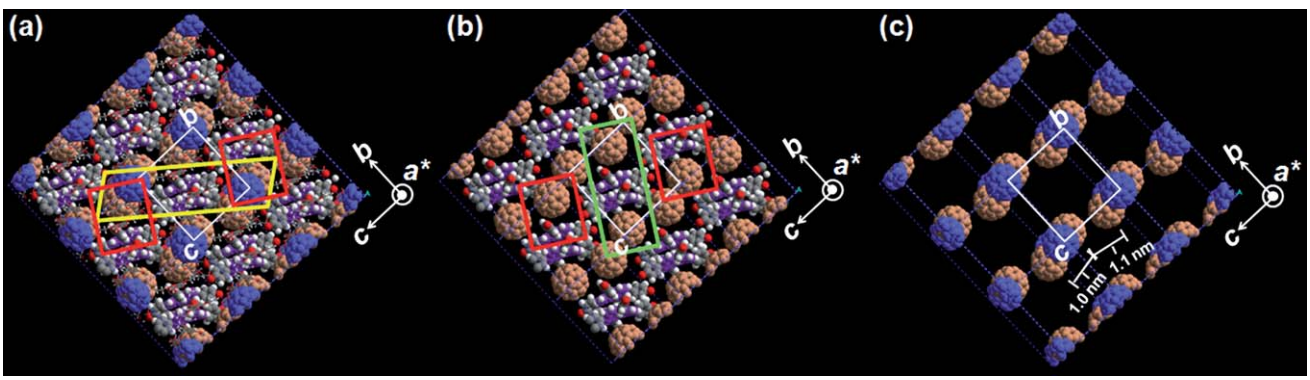

Fig. 9 (a) Space-fill molecular model with 3 × 3 unit cells viewed along the *a** axis. The yellow parallelogram indicates the motif in the unit cell. Zn(II) porphyrin cores (colored in purple) and the C_{60}s colored in brown adapt an alternating arrangement near to the [01$\bar{1}$] direction of the unit cells, while the C_{60}s colored in blue stay above and beneath, occupying the empty space around the packing. (b) Illustration of the close packing of the brown C_{60}s and Zn(II) porphyrins near to the [01$\bar{1}$] direction. (c) Illustration of the zig-zag shaped C_{60} channels along the [001] direction. Moieties are selectively omitted in (b) and (c) for clarity purpose.

C_{60} in the crystalline phase of pristine C_{60}.[55] The distances would allow a good electronic coupling among the C_{60}s, and efficient electronic properties should be expected. The continuous C_{60} channels in this supramolecular structure might thus serve as charge transport channels for the generated charge carriers. Combined with excellent thermal stability and thermal processibility, the thermotropic supramolecular donor–acceptor separated structure of diZnCPD holds promises as a component of supramolecular electronics.

Conclusions

In summary, we demonstrated the first thermotropic supramolecular structure with alternating arrangement of C_{60}s and Zn(II) porphyrins formed by a diZnCPD. The supramolecular structure includes a close packing structure of C_{60}s (acceptors) and Zn(II) porphyrins (donors) nearly along the [01$\bar{1}$] direction, and zig-zag shaped C_{60} channels along the [001] direction of its unit cell. It generates a donor–acceptor separated structure of C_{60}s and Zn (II) porphyrins in the bulk. Formation of this stable supramolecular structure is thermodynamically favorable, but kinetically difficult. Therefore, when cooled from the I phase, instead of directly transforming into the stable phase, the I phase supercooled and transformed into the less ordered, metastable phase with a layered structure. Annealing is required to finally form the stable ordered structure. In this process, the overall energy barrier of the structural formation is separated into two steps: first, to form the layered structure as the precursor and second, to construct the stable phase. The research provides a simple way to fabricate large-area supramolecular electronics based on the donor–acceptor separated supramolecular structure of C_{60}s and Zn(II) porphyrins in the solid state.

Acknowledgements

This work was supported by the National Science Foundation (DMR-0906898) and the Collaborative Center for Polymer Photonics, AFOSR. We also thank Dr Xiaopeng Li and Prof. Chrys Wesdemiotis for assistance with the MALDI-TOF mass spectra measurements.

Notes and references

1 A. J. Heeger, *Rev. Mod. Phys.*, 2001, **73**, 681.
2 A. G. MacDiarmid, *Rev. Mod. Phys.*, 2001, **73**, 701.
3 Z. Bao, A. Rogers and E. Katz, *J. Mater. Chem.*, 1999, **9**, 1895.
4 H. Sirringhaus, *Adv. Mater.*, 2005, **17**, 2411.
5 C. J. Brabec, *Sol. Energy Mater. Sol. Cells*, 2004, **83**, 273.
6 T. S. Balaban, *Acc. Chem. Res.*, 2005, **38**, 612.
7 W. Ma, C. Yang, X. Gong, K. Lee and A. J. Heeger, *Adv. Funct. Mater.*, 2005, **15**, 1617.
8 S. Günes, H. Neugebauer and N. S. Sariciftci, *Chem. Rev.*, 2007, **107**, 1324.
9 D. M. Guldi, *Phys. Chem. Chem. Phys.*, 2007, **9**, 1400.
10 A. Ajayaghosh, V. K. Praveen and C. Vijayakumar, *Chem. Soc. Rev.*, 2008, **37**, 109.
11 J. Roncali, *Acc. Chem. Res.*, 2009, **42**, 1719.
12 G. Dennler, M. C. Scharber and C. J. Brabec, *Adv. Mater.*, 2009, **21**, 1323.
13 M. R. Wasielewski, *Acc. Chem. Res.*, 2009, **42**, 1910.
14 S. Leng, B. Wex, L. H. Chan, M. J. Graham, S. Jin, A. J. Jing, K.-U. Jeong, R. M. Van Horn, B. Sun, M. Zhu, B. Kaafarani and S. Z. D. Cheng, *J. Phys. Chem. B*, 2009, **113**, 5403.
15 W. Cai, X. Gong and Y. Cao, *Sol. Energy Mater. Sol. Cells*, 2010, **94**, 114.
16 C. J. Brabec, S. Gowrisanker, J. J. M. Halls, D. Laird, S. Jia and S. P. Williams, *Adv. Mater.*, 2010, **22**, 3839.
17 S. Leng, J. Jing, L. H. Chan, J. Hu, R. M. Moustafa, R. M. Van Horn, M. J. Graham, B. Sun, M. Zhu, K.-U. Jeong, B. Kaafarani, W. Zhang, F. W. Harris and S. Z. D. Cheng, *Soft Matter*, 2010, **6**, 100.
18 X. Ren, B. Sun, C.-C. Tsi, S. Leng, Y. Tu, R. R. Kulkarni, Z. Kang, M. Zhu, W. Zhang and S. Z. D. Cheng, *J. Phys. Chem. B*, 2010, **114**, 4802.
19 F. Spanig, I. Lopez-Duarte, M. K. R. Fischer, M. V. Martinez-Diaz, P. Bauerle, T. Torres and D. M. Guldi, *J. Mater. Chem.*, 2011, **21**, 1395.
20 F. J. M. Hoeben, P. Jonkheijm, E. W. Meijer and A. P. H. J. Schenning, *Chem. Rev.*, 2005, **105**, 1491.
21 C. C. Lee, C. Grenier, E. W. Meijer and A. P. H. J. Schenning, *Chem. Soc. Rev.*, 2009, **38**, 671.
22 V. Palermo, A. Liscio, M. Palma, M. Surin, R. Lazzaroni and P. Samori, *Chem. Commun.*, 2007, 3326.
23 C. D. Simpson, J. Wu, M. D. Watson and K. Mullen, *J. Mater. Chem.*, 2004, **14**, 494.
24 A. P. H. J. Schenning and E. W. Meijer, *Chem. Commun.*, 2005, 3245.
25 R. Li, W. Hu, Y. Liu and D. Zhu, *Acc. Chem. Res.*, 2010, **43**, 529.
26 H. Liu, J. Xu, Y. Li and Y. Li, *Acc. Chem. Res.*, 2010, **43**, 1496.
27 L. C. Palmer and S. I. Stupp, *Acc. Chem. Res.*, 2008, **41**, 1674.
28 A. Ajayaghosh and V. K. Praveen, *Acc. Chem. Res.*, 2007, **40**, 644.
29 G. De Luca, E. Treossi, A. Liscio, J. M. Mativetsky, L. M. Scolaro, V. Palermo and P. Samori, *J. Mater. Chem.*, 2010, **20**, 2493.
30 P. G. A. Janssen, P. Jonkheijm, P. Thordarson, J. C. Gielen, P. C. M. Christianen, J. L. J. van Dongen, E. W. Meijer and A. P. H. J. Schenning, *J. Mater. Chem.*, 2007, **17**, 2654.
31 M. Treier, E. Orgiu, L. Zalewski, D. Cho, R. Rieger, K. Mullen and P. Samori, *J. Mater. Chem.*, 2010, **20**, 9018.
32 J. van Herrikhuyzen, P. Jonkheijm, A. P. H. J. Schenning and E. W. Meijer, *Org. Biomol. Chem.*, 2006, **4**, 1539.
33 V. Sgobba and D. M. Guldi, *Chem. Soc. Rev.*, 2009, **38**, 165.
34 A. C. Grimsdale, J. Wu and K. Mullen, *Chem. Commun.*, 2005, 2197.
35 D. M. Guldi, B. M. Illescas, C. M. Atienza, M. Wielopolski and N. Martin, *Chem. Soc. Rev.*, 2009, **38**, 1587.
36 J. Wu, A. C. Grimsdale and K. Mullen, *J. Mater. Chem.*, 2005, **15**, 41.
37 H. Ozawa, H. Tanaka, M. Kawao, S. Uno and K. Nakazato, *Chem. Commun.*, 2009, 7411.
38 S. Barrau, T. Heiser, F. Richard, C. Brochon, C. Ngov, K. van de Wetering, G. Hadziioannou, D. V. Anokhin and D. A. Ivanov, *Macromolecules*, 2008, **41**, 2701.
39 L. Biniek, S. Fall, C. L. Chochos, D. V. Anokhin, D. A. Ivanov, N. Leclerc, P. Lévêque and T. Heiser, *Macromolecules*, 2010, **43**, 9779.
40 C. Luo, D. M. Guldi, H. Imahori, K. Tamaki and Y. Sakata, *J. Am. Chem. Soc.*, 2000, **122**, 6535.
41 H. Imahori and Y. Sakata, *Adv. Mater.*, 1997, **9**, 537.
42 H. Imahori, K. Hagiwara, M. Aoki, T. Akiyama, S. Taniguchi, T. Okada, M. Shirakawa and Y. Sakata, *J. Am. Chem. Soc.*, 1996, **118**, 11771.
43 D. M. Guldi, C. Luo, M. Prato, E. Dietel and A. Hirsch, *Chem. Commun.*, 2000, 373.
44 D. M. Guldi, C. Luo, M. Prato, A. Troisi, F. Zerbetto, M. Scheloske, E. Dietel, W. Bauer and A. Hirsch, *J. Am. Chem. Soc.*, 2001, **123**, 9166.
45 P. D. W. Boyd and C. A. Reed, *Acc. Chem. Res.*, 2004, **38**, 235.
46 P. D. W. Boyd, M. C. Hodgson, C. E. F. Rickard, A. G. Oliver, L. Chaker, P. J. Brothers, R. D. Bolskar, F. S. Tham and C. A. Reed, *J. Am. Chem. Soc.*, 1999, **121**, 10487.
47 D. Sun, F. S. Tham, C. A. Reed, L. Chaker, M. Burgess and P. D. W. Boyd, *J. Am. Chem. Soc.*, 2000, **122**, 10704.
48 M. M. Olmstead, D. A. Costa, K. Maitra, B. C. Noll, S. L. Phillips, P. M. Van Calcar and A. L. Balch, *J. Am. Chem. Soc.*, 1999, **121**, 7090.
49 C. M. Drain, A. Varotto and I. Radivojevic, *Chem. Rev.*, 2009, **109**, 1630.
50 T. Yamaguchi, N. Ishii, K. Tashiro and T. Aida, *J. Am. Chem. Soc.*, 2003, **125**, 13934.
51 V. Georgakilas, F. Pellarini, M. Prato, D. M. Guldi, M. Melle-Franco and F. Zerbetto, *Proc. Natl. Acad. Sci. U. S. A.*, 2002, **99**, 5075.
52 D. Sun, F. S. Tham, C. A. Reed and P. D. W. Boyd, *Proc. Natl. Acad. Sci. U. S. A.*, 2002, **99**, 5088.

53 L. A. K. Staveley, *Annu. Rev. Phys. Chem.*, 1962, **13**, 351.
54 J. Timmermans, *J. Chem. Phys.*, 1938, **35**, 331.
55 P. A. Heiney, J. E. Fischer, A. R. McGhie, W. J. Romanow, A. M. Denenstein, J. McCauley, A. B. Smith and D. E. Cox, *Phys. Rev. Lett.*, 1991, **66**, 2911.
56 D. Demus, J. Goodby, G. W. Gray, H.-W. Spiess, and V. Vill, *Handbook of Liquid Crystals*, Wiley-VCH, Weinheim, 1998, vol. 2A.
57 X. Zhou, S. W. Kang, S. Kumar, R. R. Kulkarni, S. Z. D. Cheng and Q. Li, *Chem. Mater.*, 2008, **20**, 3551.
58 S. Sergeyev, W. Pisula and Y. H. Geerts, *Chem. Soc. Rev.*, 2007, **36**, 1902.
59 S. Laschat, A. Baro, N. Steinke, F. Giesselmann, C. Hagele, G. Scalia, R. Judele, E. Kapatsina, S. Sauer, A. Schreivogel and M. Tosoni, *Angew. Chem., Int. Ed.*, 2007, **46**, 4832.
60 D. Felder, H. Nierengarten, J. P. Gisselbrecht, C. Boudon, E. Leize, J. F. Nicoud, M. Gross, A. V. Dorsselaer and J. F. Nierengarten, *New J. Chem.*, 2000, **24**, 687.
61 S. Z. D. Cheng, Z. Wu, M. Eashoo, S. L. C. Hsu and F. W. Harris, *Polymer*, 1991, **32**, 1803.
62 M. Eashoo, Z. Wu, A. Zhang, D. Shen, C. Tse, F. W. Harris, S. Z. D. Cheng, K. H. Gardner and B. S. Hsiao, *Macromol. Chem. Phys.*, 1994, **195**, 2207.
63 R. Pardey, A. Zhang, P. A. Gabori, F. W. Harris, S. Z. D. Cheng, J. Adduci, J. V. Facinelli and R. W. Lenz, *Macromolecules*, 1992, **25**, 5060.
64 R. Pardey, D. Shen, P. G. Gabori, F. W. Harris, S. Z. D. Cheng, J. Adduci, J. V. Facinelli and R. W. Lenz, *Macromolecules*, 1993, **26**, 3687.
65 R. Pardey, S. S. Wu, J. Chen, F. W. Harris, S. Z. D. Cheng, A. Keller, J. Aducci, J. V. Facinelli and R. W. Lenz, *Macromolecules*, 1994, **27**, 5794.
66 S. Z. D. Cheng and A. Keller, *Annu. Rev. Mater. Sci.*, 1998, **28**, 533.
67 A. Keller and S. Z. D. Cheng, *Polymer*, 1998, **39**, 4461.
68 S. Z. D. Cheng, in *Phase Transitions in Polymers, The Role of Metastable State*, Elsevier Science B.V., 2008.
69 V. A. Luchnikov, D. V. Anokhin, S. Z. D. Cheng, C.-L. Wang, G. Bar and D. A. Ivanov, *J. Appl. Crystallogr.*, 2011, **44**, 540.
70 D. V. Anokhin, R. I. Gearba, Yu. K. Godovsky, S. N. Magonov, N. N. Makarova, R. I. Ivanov, W. Bras and D. A. Ivanov, *Polymer*, 2007, **48**, 4837.
71 G.-H. Kim, C. Pugh and S. Z. D. Cheng, *Macromolecules*, 2000, **33**, 8983.